Title

Critical Mechanistic Role of Inositol Hexakisphosphate (IP6) in HIV-1 Viral Capsid Assembly

Authors

Manish Gupta, Alexander J. Pak,[⊥] and Gregory A. Voth[*]

Affiliations

Department of Chemistry, Chicago Center for Theoretical Chemistry, Institute for Biophysical Dynamics, and James Franck Institute, The University of Chicago, Chicago, IL 60637, United States

[⊥]Present address: Department of Chemical and Biological Engineering, Colorado School of Mines, Golden, CO 80401, United States

[*]Corresponding author: gavoth@uchicago.edu

Abstract

The maturation of HIV-1 capsid protein (CA) into a cone-shaped lattice encasing the condensed RNA genome is critical for viral infectivity. CA can self-assemble into a wide range of capsid morphologies made of ~175-250 hexamers and exactly 12 pentamers. Most recently, cellular polyanion inositol hexakisphosphate (IP6) has been demonstrated to facilitate conical capsid formation by coordinating a ring of arginine residues within the central cavity of capsid hexamers and pentamers. However, the precise interplay of events during IP6 and CA co-assembly is unclear. In this work, we use Coarse-Grained Molecular Dynamics (CGMD) simulations to elucidate the underlying molecular mechanism that allows IP6 to have crucial roles in HIV-1 maturation. We show that IP6 promotes curvature generation by trapping pentameric defects in the growing lattice and shifts assembly behavior towards kinetically favored outcomes. Our analysis suggests that IP6 can stabilize metastable capsid intermediates and may induce structural pleomorphism in mature capsids.

Teaser

Coarse Grained simulations reveal that IP6 promote fullerene-like capsid formation by stabilizing high curvature regions of the capsid.

Introduction

The HIV-1 replication process requires budding of immature viral particles that subsequently undergo a crucial structural rearrangement called maturation.[1,2] HIV-1 maturation is a string of biochemical and morphological changes induced by proteolytic processing of Gag by viral protease (PR),[1,3] leading to self-assembly of released capsid protein (CA) into a cone-shaped capsid[4] (mature core) encasing a dense RNA/Nucleocapsid (NC) complex.[5] The mature capsid executes several critical functions during reverse transcription (RT)[6], cellular trafficking[7] and nuclear import.[8,9] Thus, mature capsid generation is essential for HIV-1 infection, with failure resulting in loss of viral infectivity.[10-12]

The CA monomer contains two independent domains, the N-terminal domain (NTD) comprising seven α-helices and a β-hairpin and the C-terminal domain (CTD) comprising four α-helices, that are connected by a flexible linker[13]. Interestingly, CA can adopt a dimeric form (Fig. 1a) in solution due to interactions between CTD helices[13,14] and exists in a dynamic monomer/dimer equilibrium.[14] CA can self-assemble into a wide variety of morphologies while a typical capsid is a closed fullerene shell (Fig. 1d), composed of hexamer and pentamer building blocks (Fig. 1c) with more than 1000 copies of CA.[4,15] Typical HIV-1 virions contain 2500-5000 Gag monomers in a non-trivial and highly crowded environment.[16-19] Therefore, a mature capsid, which contains only half of the CA present in an immature virion, exists in equilibrium with solution state CA. As the assembly condition is sensitive to variation in CA concentration, pH and salt concentration, biochemical reconstitution of CA assembly has been particularly challenging.[20] Under favorable conditions, a mixture of cone and cylinder formation was observed in most of the previous *in vitro* studies.[21,22] Cryo-EM and image reconstruction studies have identified several key structural motifs for capsid assembly that involve interactions between NTD/NTD, NTD/CTD and CTD/CTD interfaces of CA.[23,24] Characterization of CA tubular assemblies showed that the NTDs form a hexagonal arrangement while inter-hexamer CTD interfaces connect adjacent assembly units.[23] Based on various *in vitro*[23,24] and intact virion[25] analyses, the atomic structure of mature cores, following a fullerene cone model, with exactly 12 pentamers[22,24,26] in agreement with Euler's theorem, has also been determined. Recent X-ray crystallography studies reveal that a narrow pH gated pore with a ring of R18 at its center is distributed throughout the capsid surface.[27,28] This ring of R18 is essential for RT and avidly binds several host cell metabolites.[27] Interestingly, HIV-1 package more than 300 molecules of negatively charged IP6 per virion[29] which is already known to influence immature Gag assembly.[29,30] Pioneering work by Dick *et al*. demonstrated that IP6 is also critical for enhanced assembly of cone-shaped mature cores.[31] IP6 has been shown to interact with the

ring of R18 and removal of electropositive repulsion in the central pore by R18A mutation precludes viral infectivity.[31] Therefore, it is evident that IP6 plays a central role in infectious capsid formation. In a previous work, the structural basis for interaction between IP6 and capsid building blocks was illustrated using all-atom (AA) molecular dynamics (MD). Free energy calculations indicated that IP6 preferentially stabilizes CA pentamers over hexamers.[32] Therefore, we hypothesize that IP6 promotes capsid formation by stabilizing pentamers, which are necessary for inducing curvature in the capsid. However, the detailed molecular mechanism of IP6 and CA co-assembly and several important questions regarding the mechanism of pentamer inclusion and curvature generation during the HIV-1 self-assembly remain elusive.

All-atom simulations offer complementary insight to experimental studies. AAMD simulations of full-capsid have revealed several key physical and chemical properties of capsid dynamics and structure,[33,34] nonetheless, these techniques are computationally exorbitant and, therefore, inadequate for studying the large-scale functional dynamics of assembly processes that occur over long time scales. Alternatively, Coarse-grained (CG) approaches reduce system complexity to a simpler molecular description while retaining the ability to predict emergent behavior.[35] While caution should be exercised when considering large-scale molecular assembly, general agreement with experimental results is often considered a reliable indicator of CG model fidelity. Our previous CG simulations offered valuable insight into the effects of CA conformational freedom, concentration and molecular crowding on self-assembly[36,37] explaining the initial stages of capsid growth. In this work, however, we extend our prior CG model[36] to include and, investigate the effects of IP6 on HIV-1 capsid formation. In particular, we examine the kinetic pathways promoted by IP6 that lead to capsid morphogenesis. We observe that IP6 is essential for formation of high curvature lattice regions representing kinetically favored intermediates. We propose that the physiological role of IP6 is to induce curvature by stabilizing pentamers during self-assembly.

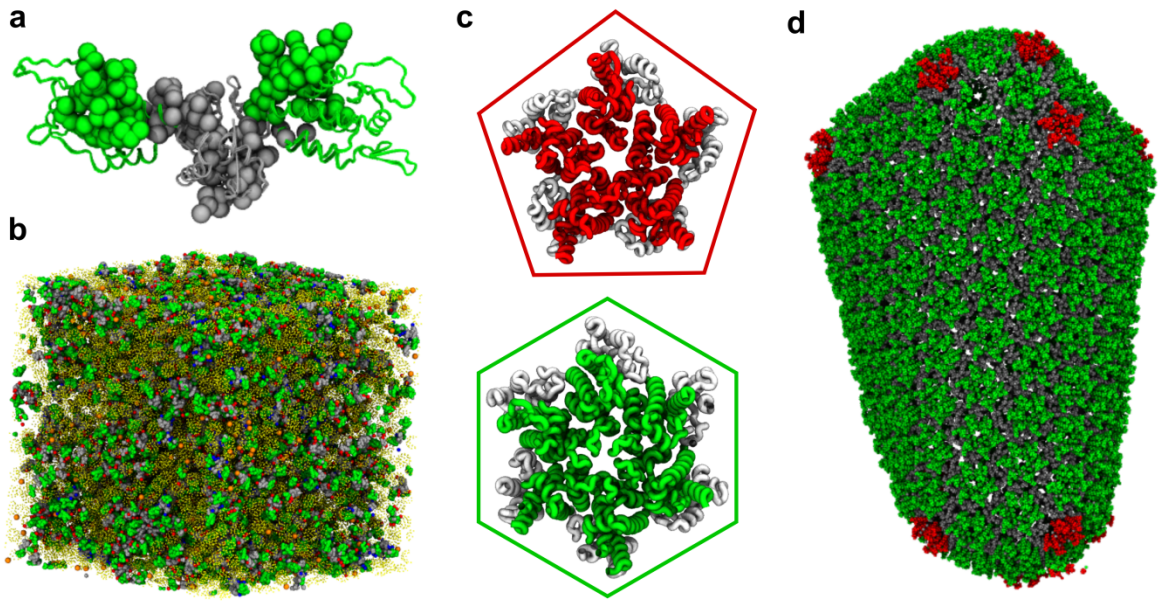

Figure 1. CG model of HIV-1 CA dimer and CGMD simulation setup. (a) Overlay of a CG CA dimer (NTD green and CTD gray) over an all-atom CA dimer (PDB 2ML8).[14] (b) Snapshot of an initial simulation setup; CA dimer (green, gray beads and blue/red for active/inactive), IP6 (orange beads), inert crowder (transparent yellow). (c) Quasi-equivalent pentamers (PDB 3P05) and hexamers (PDB 5HGL) after ref 15 and 26 respectively. CTDs are gray and NTDs are red for capsid pentamer and green for hexamer. (d) Mature core is made of Pentamer (red) and Hexamer (green) building blocks.

Results

CA assembly behavior in the absence of IP6

HIV-1 CA monomers consist of two globular domains (NTD and CTD) connected by a flexible linker. The monomer is conformationally flexible and adopts an assembly competent (i.e. mature-like) state ($[CA]_+$) with only 5-10% probability in solution.[14] To emulate this behavior in our CG simulations, CA was partitioned into assembly competent ($[CA]_+$) and assembly incompetent ($[CA]_-$) populations and all free CA were periodically assigned to either the $[CA]_+$ or $[CA]_-$ state with a fixed $[CA]_+$ probability; the state switching rate was chosen to maintain assembly relevant correlation times (conformational switching interval), i.e. inter-domain motions. During the assembly process, CA forms dimers that then associate with the growing lattice to form the complete capsid shell.[36] Several *in vitro* experiments demonstrate that, in the absence of IP6, CA predominantly forms hollow tubes made of hexamers.[24,31] While our prior

CG model[36] of CA predicted cone formation, we tested whether our CG model was also capable of producing tubes, resulting in a mixed population of tubes and cones. To simulate CA assembly, 4 independent trajectories with 600 CA dimers were propagated for 5×10^8 CG steps and 200 mg/mL inert crowder density with $[CA]_+$ = 15% and conformational switching interval of 5×10^5 time steps. The CA concentrations in our simulations were about 50% of a typical virion due to computational expense. However, by increasing $[CA]_+$ to 15% in comparison to our prior studies[36,38] that used $[CA]_+$ = 10%, we compensate for the possible undersupply of assembly competent CA. From our CG simulations, we observed 3 tubular structures and 1 truncated cone (Fig. 2a and S1). CA dimers quickly produced metastable trimer of dimer populations ($< 5 \times 10^6$ CG steps), but nucleation of these trimers was slow and did not occur before 10^7 CG steps. The growing lattice curled into a hollow cylinder and grew rapidly by CA dimer association at both ends generating a sheet of hexamers (Fig. 2a). After 2×10^8 CG steps, pentamer defect incorporation at the edge of the lattice was observed forming a narrow end. Interestingly, CA self-assembly at the exposed lattice edges was dynamic and exhibited a degree of local remodeling by error correction. The other end of the CA tube continued to grow until the population of assembly competent CA was exhausted in the simulation box. As shown in Fig. 2b, the final CA tube containing 845±40 CA monomers was primarily composed of hexamers (126±7). The diameter of the final structure was 38 ± 6 nm, which is consistent with tube diameters from *in vitro* experiments.[23] The rarer appearance of truncated cones (Fig. S1) reflects the ability of our CA model to assemble spontaneously into both helical tubes and cones with a preference for tubular structures in the absence of IP6.

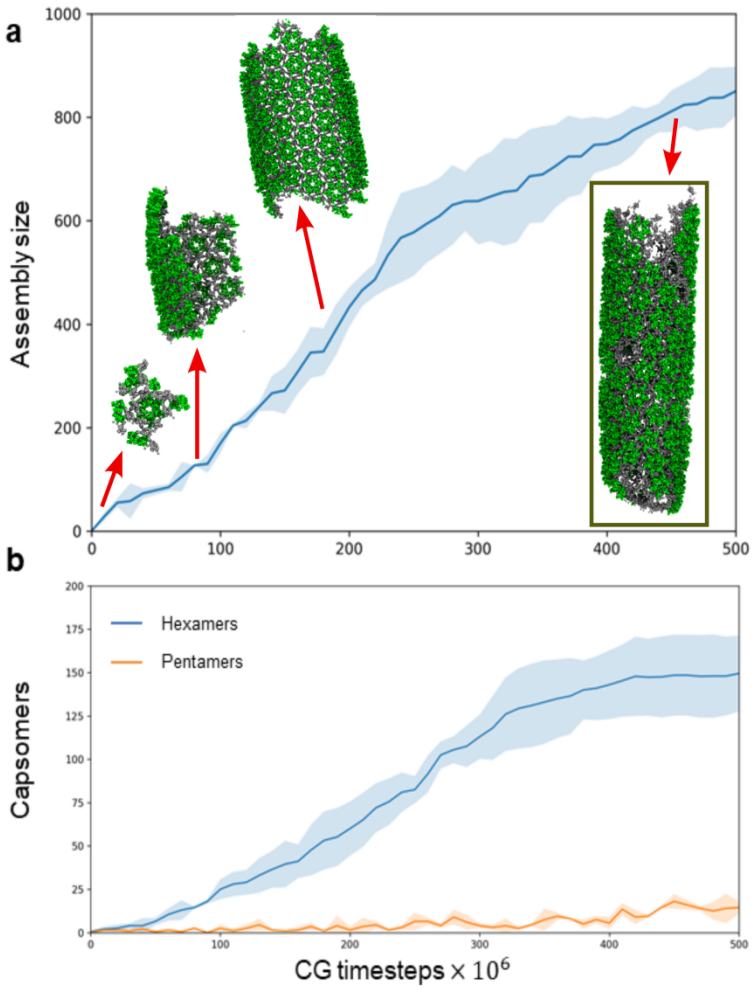

Figure 2. CGMD simulations of CA dimer assembly in the absence of IP6. (a) Assembly time-series plot that depicts cluster size as a function of CG time. CA dimers preferably assemble into tubular structures in the absence of IP6 (CA NTDs are green and CTDs are gray). Simulation snapshots taken at 10×10^6, 100×10^6, 200×10^6, 450×10^6 CG time steps. (b) Time-series profile of the total number of hexamers and pentamers as a function of CG time step. In both panels, the shaded region represents the standard deviation across all four replicas.

Molecular mechanism of IP6 mediated CA assembly

Recent studies have shown that the negatively charged host metabolite IP6 can stabilize the six helix-bundle[31] in the immature Gag and is efficiently recruited by HIV-1 virions.[39] After proteolysis, IP6 is known to stabilize the mature capsid by binding at the central ring of R18.[32] IP6 is also critical for enhanced mature capsid formation.[31] Thus, IP6 shifts the population of assembled CA morphologies towards mature capsid cones through as-yet unknown mechanisms. A typical mature capsid contains 1000-1500 CA monomers.[4,15] Therefore, we

increased the simulation box domain to 90×90×90 nm^3 with 880 CA dimers to allow the formation of complete capsids. To examine the effects of IP6 during self-assembly, simulations were performed with 4mM CA and 600 IP6 molecules using the aforementioned assembly conditions, including the concentration of inert crowders and the CA conformational switching rate. Figure 3 presents different stages of IP6 mediated capsid assembly. A small and curled hexameric lattice formed initially with small curvature since the dihedral angle between adjacent hexamer-hexamer planes were close to 180°. This explains the formation of the flat middle region in the initial stages of capsid assembly (~1.7×10^8 CG steps). Subsequently, stable pentamers formed at the broad end of the capsid and were stabilized by IP6, imparting curvature to the capsid shell. The growth of the capsid lattice followed a sigmoidal profile, a characteristic also observed experimentally.[40] Interestingly, the narrow cone formed last in our simulations where five proximal pentamers emerged, leading to the high-curvature cap shown in Figure 3.

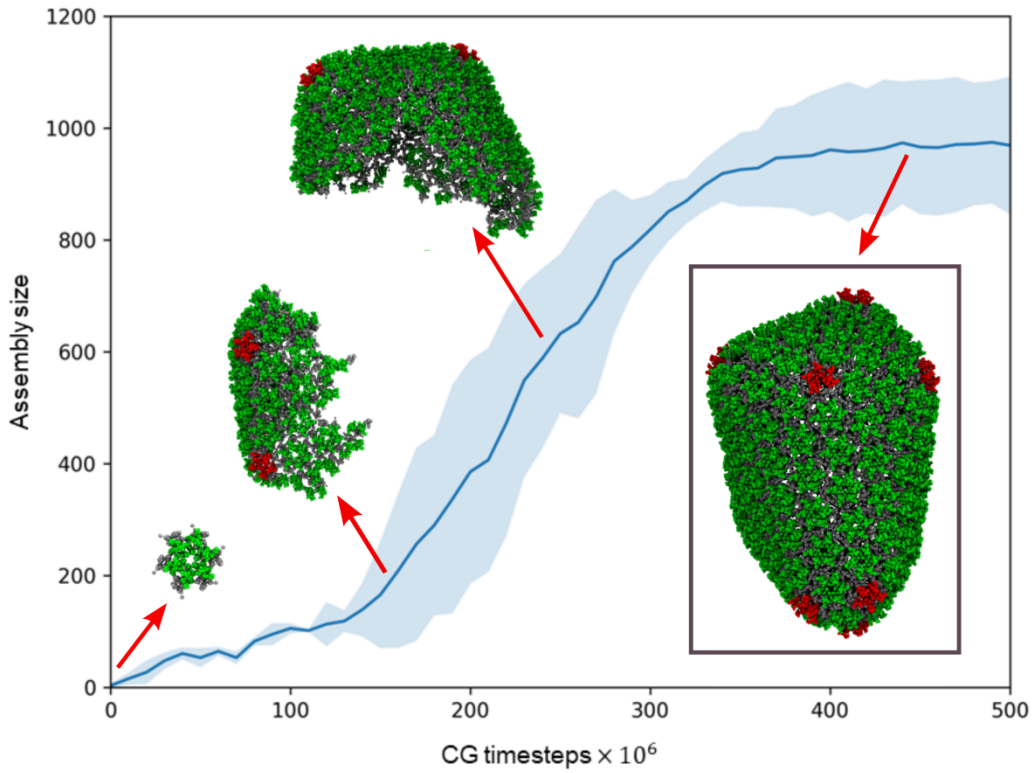

Figure 3. CGMD simulations of CA dimer assembly in the presence of IP6. (a) Time-series plot of assembled lattice size as a function of CG time step. CA dimers assemble into a conical capsid in the presence of IP6 (CA hexamer NTDs are green, pentamer NTDs are red and all CTDs are gray).

Simulation snapshots taken at 10×10^6, 125×10^6, 250×10^6, 450×10^6 CG time steps. The shaded region represents the standard deviation across six replicas.

The complete capsid contained 978±121 CA subunits and was observed after 5×10^8 CG steps. We analyzed time series profiles of CG trajectories in Figure 4, in which we find that the complete capsid core is composed of 151±21 CA hexamers and exactly 12 pentamers. To further understand the role of IP6 in CA assembly kinetics, we counted the number of IP6 bound capsid hexamers and pentamers. While IP6 bound with only 15-20% of the hexamers, atleast 50% of the pentamers were bound with IP6 (Fig. 4a & b), indicating that IP6 shows preference towards pentamers in our simulations.

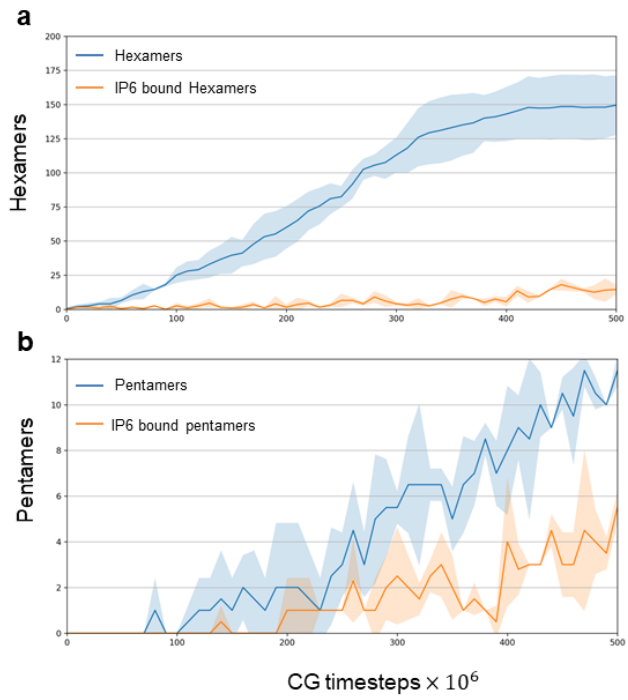

Figure 4. Assembly time-series profiles illustrate the preference of IP6 towards pentamers over hexamers. (a) The total number of hexamers and the total number of IP6 bound hexamers in the capsid as a function of CG time, (b) The total number of pentamers and the total number of IP6 bound pentamers in the capsid as a function of CG time. In both panels, the shaded region represents the standard deviation across six replicas.

IP6 accelerates CA assembly rate and stabilizes regions of high curvature

To further investigate the precise role of IP6 in CA assembly, we compared the early stages of assembly in the absence and presence of IP6. We performed 10 additional short

simulations, 5 each for CA without IP6 and CA with IP6 starting from a pre-nucleated hexameric cluster with 6 CA dimers. We depict the assembly rate of CA in Figure 5 and analyze the two cases. In the presence of IP6, the assembled clusters contain 150±44 CA monomers after 5×10^7 CG steps. During the early stages of assembly, IP6 binds with the nucleated cluster and accelerates CA assembly compared to that of the IP6-absent condition. While local remodeling at the growing lattice edges is a key feature of capsid assembly, we observed that IP6 binding stabilizes defects in capsid intermediates, thereby, curtailing extensive error correction and facilitating CA association.

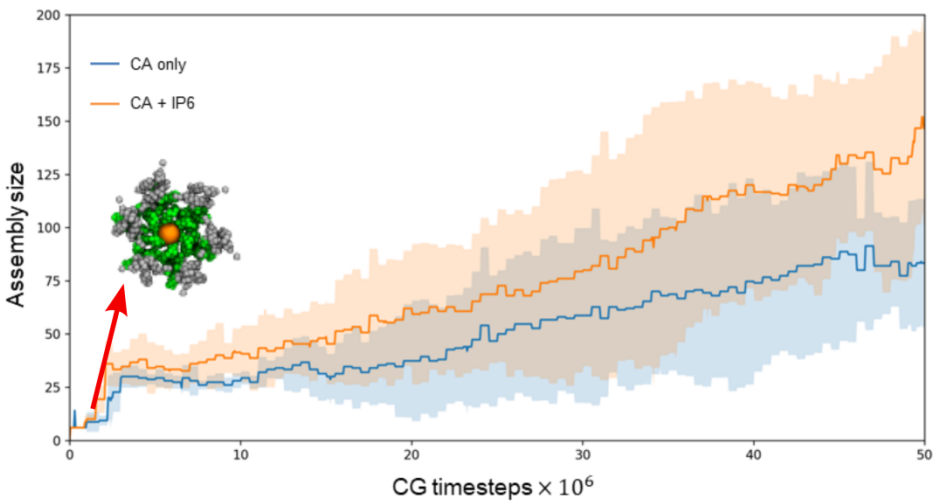

Figure 5. IP6 accelerates CA assembly rate by kinetically trapping capsid intermediates (colour scheme is same as Figure 3. IP6 is orange). Time series profiles of cluster size as a function of CG time step in the presence and absence of IP6. In both panels, the shaded region represents the standard deviation across five replicas.

It has been mentioned that HIV-1 capsids possess a caged polyhedral arrangement composed of CA hexamers and exactly 12 pentamers.[4,24] These pentamers introduce curvature on the capsid and are necessary for capsid closure. On the basis of 2.5 Å X-ray crystallography structures, hexamers and pentamers were determined to be quasi-equivalent[15] with the positively charged R18 sidechains throughout the central pore juxtaposed more closely in the pentamer compared to the hexamer yielding stronger electrostatic repulsion in the former. Pentamers are considered defects and are disfavored compared to regular hexamers. Our CA simulations also show a certain degree of error correction where defective pentamers are

annealed into hexamers. Intriguingly, the high curvature regions both at the broad and narrow ends of the capsid had more IP6 population than the comparatively flatter middle region as shown in Figure 6.

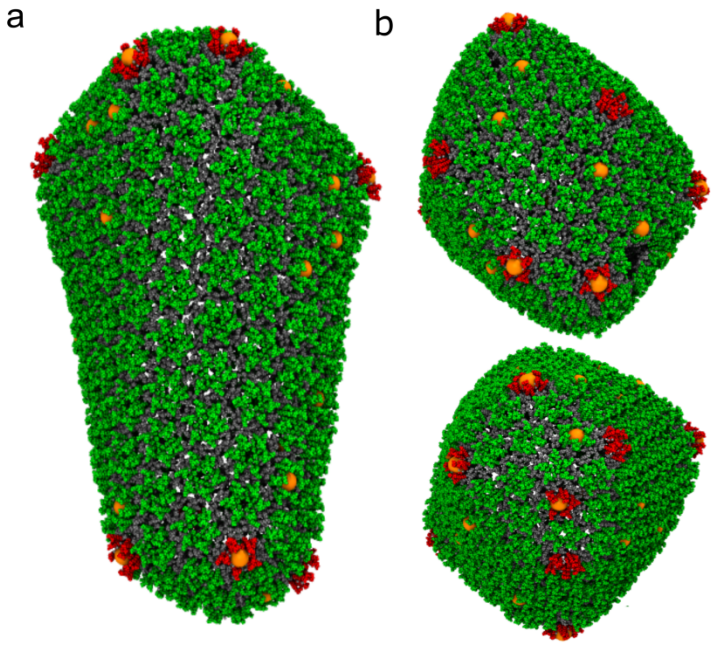

Figure 6. CGMD simulations reveal that IP6 stabilizes the capsid by binding at regions of high curvature. (a) Side view of capsid (Colour scheme is same as Figure 3. (b) Top and bottom view.

We observed that IP6 prefers binding to the regions of high curvature and are responsible for lattice curvature generation. It should be noted that only 15 to 35 IP6 molecules intercalated with capsid shell during CA assembly and IP6 binding continued even after full capsid formation (Fig 4). Recent experimental studies show that the narrow end of the HIV-1 core may not close if the conditions are not favorable.[41] However, all capsids generated during our simulations closed completely suggesting that IP6 assists in closure by stabilizing pentamers which accommodate curvature at regions of high stress.

IP6 stabilization of capsid intermediates determines mature virion morphology

The fullerene core is a defining feature of HIV-1 maturation.[3] However, it is not unusual for HIV-1 viral capsids to display morphological diversity.[21,25,40,42,43] Depending on the spacing between pentameric defects, capsid cores adopt a wide distribution of cone angles thereby producing different morphologies. Analogously, the variable distribution in capsid sizes is suggestive of a robust assembly process. Figure 7 presents different morphological outcomes during our simulations of CA self-assembly with IP6. We observed that curvature generation in capsid intermediates was dictated by stabilization of pentameric defects by IP6. Early

incorporation of these pentameric defects resulted in smaller cores (Figure 3 and 7b), whereas, timely pentamer incorporation into the extended hexagonal lattice led to appropriate curvature generation for relatively larger mature core formation as shown in Figure 7a,c,e.

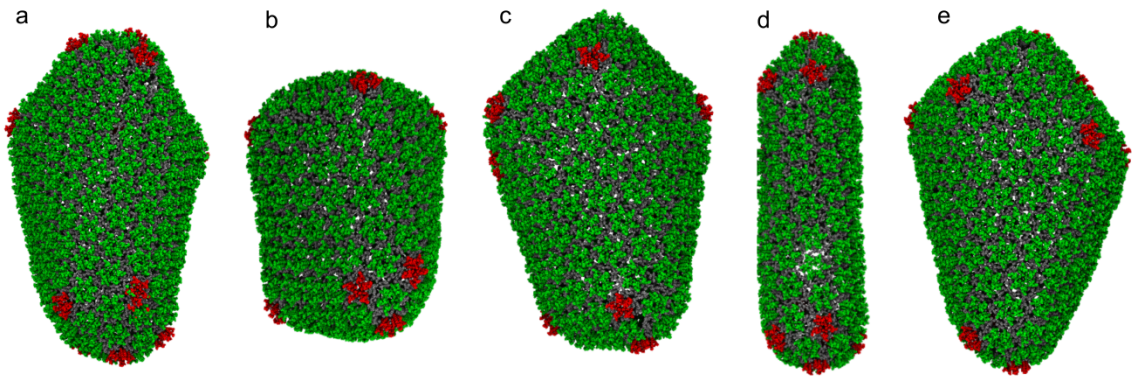

Figure 7. IP6 promotes capsid pleomorphism. (a-e) Snapshots of final structures from five additional CGMD simulations in the presence of IP6 (CA colour scheme as in Figure 3). IP6 molecules stabilize lattice curvature inducing the formation of kinetically trapped structural outcomes.

Discussion

We use CGMD simulations to elucidate the critical role of IP6 during HIV-1 capsid self-assembly. Our CG simulations capture assembly behavior at time and length scales relevant for viral capsid morphogenesis and generate virion relevant morphologies suggesting that CG simulations can provide crucial insight into CA assembly kinetics. While RNA complex is known to promote capsid nucleation,[26] it should be noted that simulations presented here assume that RNA is not essential for capsid formation, which is in agreement with recent experiments that indicate cone formation can be achieved in the absence of RNA.[44] In the absence of IP6, we find that mature CA assembly is self-regulated through efficient error-correction, leading to tubule formation. This ensures increased contact among CA monomers and removal of transient pentamer defects by local remodeling, suggesting that, CA assembly nominally proceeds through a thermodynamically-driven pathway producing near-equilibrium structures. However, depending on the local $[CA]_+$ concentration and crowding, lattice growth can be too rapid for error correction, leading to conical structures with stable pentamers embedded within the lattice as seen occasionally in our simulations and select *in vitro* experiments.[22] This explains the primary formation of cylinders and the rarer occurrence of cone-shaped mature cores in the absence of IP6.

The morphological transition from an immature spherical Gag lattice to mature core is not well understood but there are two competing models for this transformation, the disassembly/reassembly model[45] and the displacive mechanism.[46,47] Evidence in support of the disassembly/reassembly model includes several structural studies demonstrating distinct lattice spacings and different protomer-protomer contacts between the immature and mature shells.[5,48] Alternatively, the displacive transition of CA-SP1 mutants with cleavage defects into mature cores support the displacive model.[47] Recent *in vitro* experiments and computer simulations indicate a sequential combination of both displacive and disassembly/reassembly pathways during capsid maturation[49] where the growth of nucleated CA proceeds through initial formation of the broad capsid followed by capsid closure at the narrow end.[50,51] Our simulations explore the basis of IP6 mediated capsid growth and closure which is relevant for both sequential displacive and disassembly/reassembly pathway and CA assembly under *in vitro* conditions. It is unclear why viral capsids assume conical morphologies with pentameric defects over more stable cylinders. In the absence of IP6, pentamers are unstable and eventually get annealed into hexamers, as evidenced by fluctuation in pentamer population in our simulations (Fig. 2b), while in the presence of IP6, a combined effect of accelerated assembly and pentamer stabilization allows formation of exactly 12 stable pentamers. However, we note that, over our simulation timescales, not all pentamers bind to IP6, indicating only a few pentamers stabilized by IP6 are sufficient to facilitate curvature generation and subsequent pentamer formation. This also explains tube formation under low concentrations of IP6 *in vitro*.[31] Cone formation may be difficult to accomplish at low concentrations of IP6 due to the stochastic nature of pentamer trapping by IP6 intercalation. It should be noted that our simulations predict additional IP6 intercalation even after full capsid formation. Our simulations suggest a delicate balance between curvature generation and lattice growth during CA self-assembly. Therefore, depending on the extent of capsid growth achieved before the inclusion of pentamers necessary for capsid closure, mature capsids may contain 1000-1500 CA monomers, explaining the heterogeneity in capsid shape and size.[21]

Interestingly, a single CA protein is capable of a wide conformational flexibility, as evident by the range of morphologies with varied curvature in expressed and purified capsids.[24,52] Computational modeling studies of the HIV-1 capsid revealed that pentameric declination hinges upon flexibility in the CTD-CTD dimer interface[15] whereas the NTD-CTD interface is believed to modulate variable lattice curvature in both hexamer and pentamer by limiting the movement of CA-CTD with respect to CA-NTD.[42] Nonetheless, the free energy penalty for sharp lattice curvature formation, as seen in some of non-canonical capsid

morphologies, can be prohibitive as evident from the ubiquitous appearance of CA cylinders in the absence of IP6. In our simulations, IP6 molecules stabilize capsid intermediates thereby enabling the formation of high curvature regions and relatedly promoting non-canonical core formation. We speculate small molecules that target IP6 binding sites can preclude HIV-1 viral infectivity by inducing early capsid closure by rapid incorporation of pentamer defects or by overstabilizing the capsid.[38] Considering the hierarchical nature of capsid assembly, our results underscore the IP6 binding site as a target of opportunity and can provide valuable insights into the development of potential maturation inhibitors. It is of note to recognize that the need for efficient and authentic assembly imparts extreme genetic fragility on HIV-1 CA.[53] However, the current CG model is derived from experimental phenomenology which is incapable of providing detailed chemically-specific insights or electrostatic interactions and, therefore, is unable to explore CA sequence mutation related variation in assembly property. Further simulations that probe the basis of assembly behavior of CA variants will likely require incorporation of all-atom statistics recapitulating the configuration space of protein mutation. Additionally, the recruitment of nucleotides into the positively charged cavity of R18 is absolutely essential for reverse transcription. Since IP6 plays important role in stabilizing the ring of R18, additional CG simulations that target the role of IP6 in nucleotide recruitment and import at the virion level will be crucial to understand the conformity of capsid pore as a potential drug target.

Materials & Methods

CG model details and simulations. The NTD and CTD of a CA CG monomer were represented as independent elastic network models (ENMs) containing Cα atoms from CA α–helices, while a weak ENM maintained inter-domain connections. An excluded volume potential with an effective radius of was used to prevent unphysical overlaps between CG beads. Important CA protein/protein interfaces were represented by attractive interactions which can be enabled and disabled, generating assembly competent ($[CA]_+$) and assembly incompetent ($[CA]_-$) CA populations. Inert crowding agents represented the effective size of Ficoll 70 through excluded vlume interactions.[40] Full details of the CG models for CA and the inert crowding agent are described in ref 36. We generated a single site CG model for IP6 using a linear center-of-mass mapping. Interactions between CA and IP6 are represented by an attractive interaction, with the locations of energy minima parameterized using a CG model of the full capsid. CA self-assembly process is highly sensitive to the specifics of local environment. In addition to that, difficulty in accurate representation of the weak binding effects between proteins and dynamics of IP6 binding with growing lattice in virion-relevant conditions

renders CG parameterization difficult. The attractive interaction between the R18 residue of CA and IP6 was represented by a Gaussian potential $\frac{H}{\sigma\sqrt{2\pi}}\exp\left[-\frac{(r_{jk}-r_0)^2}{2\sigma^2}\right]$, where r_0 is the location of energy minima. The parameter H and σ describe the depth and width of the Gaussian energy well. All simulations were prepared using Moltemplate.[54] For the CA self-assembly simulations, 1232 monomers, 1700 inert crowders were randomly distributed throughout a 80×80×80 nm^3 cubic box with periodic boundaries; four replicas were simulated. Another distinct system using a 90×90×90 nm^3 cubic box with periodic boundaries and with 1760 CA and 2496 inert crowders was prepared for comparing the assembly rates of CA; five replicas were simulated. For the CA and IP6 co-assembly simulations, a random distribution of 1760 CA, 600 IP6 molecules and 2496 inert crowders were prepared in a 90×90×90 nm^3 cubic box with periodic boundaries; six replicas were simulated. All CG MD simulations were performed using LAMMPS 21Jul2020.[55] All simulations were performed in a constant NVT ensemble using a Langevin thermostat[56] at 300 K with a damping period of 100 ps and timestep τ = 10 fs. $[CA]_+/[CA]_-$ UCG state switching was attempted every 5×10^5 τ. For all simulations, a swarm of 50 parallel independent trajectories were propagated for 10^7 τ initially to expedite the identification of a nucleated cluster. The trajectory yielding a nucleated cluster (size < 12 CA monomers) was used to initialize the production runs. Simulation snapshots were saved every 10^7 τ.

Data analysis and visualization. Graph analysis of assembled lattices was performed using the Python package NetworkX 2.1 (http://networkx.github.io/) using two proximity criteria. Inter-hexameric contacts were defined by the CTD dimer interface, i.e. when the distance between CG types 102/102 were less than 2.5 nm. Intra-hexameric contacts were defined by the distance between CA R18, i.e. when CG types 2/2 were less than 1.4 nm. Time series profiles of extracted clusters were generated using Python package Matplotlib.[57] Visualization of extracted clusters were generated using VMD 1.9.3.[58]

References

1 W. I. Sundquist and H. G. Kräusslich. "HIV-1 assembly, budding, and maturation", Cold Spring Harb Perspect Med **2**, a006924 (2012).

2 B. K. Ganser-Pornillos, M. Yeager and W. I. Sundquist. "The structural biology of HIV assembly", Curr Opin Struct Biol **18**, 203-217 (2008).

3 E. O. Freed. "HIV-1 assembly, release and maturation", Nat Rev Microbiol **13**, 484-496 (2015).

4 B. K. Ganser, S. Li, V. Y. Klishko, J. T. Finch and W. I. Sundquist. "Assembly and analysis of conical models for the HIV-1 core", Science **283**, 80-83 (1999).

5 J. A. Briggs and H. G. Kräusslich. "The molecular architecture of HIV", J Mol Biol **410**, 491-500 (2011).
6 V. B. Shah, J. Shi, D. R. Hout, I. Oztop, L. Krishnan, J. Ahn, M. S. Shotwell, A. Engelman and C. Aiken. "The host proteins transportin SR2/TNPO3 and cyclophilin A exert opposing effects on HIV-1 uncoating", J Virol **87**, 422-432 (2013).
7 E. Toccafondi, D. Lener and M. Negroni. "HIV-1 Capsid Core: A Bullet to the Heart of the Target Cell", Frontiers in Microbiology **12** (2021).
8 C. Liu, J. R. Perilla, J. Ning, M. Lu, G. Hou, R. Ramalho, B. A. Himes, G. Zhao, G. J. Bedwell, I.-J. Byeon, J. Ahn, A. M. Gronenborn, P. E. Prevelige, I. Rousso, C. Aiken, T. Polenova, K. Schulten and P. Zhang. "Cyclophilin A stabilizes the HIV-1 capsid through a novel non-canonical binding site", Nature Communications **7**, 10714 (2016).
9 A. J. Price, A. J. Fletcher, T. Schaller, T. Elliott, K. Lee, V. N. KewalRamani, J. W. Chin, G. J. Towers and L. C. James. "CPSF6 Defines a Conserved Capsid Interface that Modulates HIV-1 Replication", PLOS Pathogens **8**, e1002896 (2012).
10 T. Dorfman, A. Bukovsky, A. Ohagen, S. Höglund and H. G. Göttlinger. "Functional domains of the capsid protein of human immunodeficiency virus type 1", Journal of Virology **68**, 8180-8187 (1994).
11 F. Mammano, A. Ohagen, S. Höglund and H. G. Göttlinger. "Role of the major homology region of human immunodeficiency virus type 1 in virion morphogenesis", J Virol **68**, 4927-4936 (1994).
12 U. K. von Schwedler, K. M. Stray, J. E. Garrus and W. I. Sundquist. "Functional surfaces of the human immunodeficiency virus type 1 capsid protein", J Virol **77**, 5439-5450 (2003).
13 J. R. Perilla and A. M. Gronenborn. "Molecular Architecture of the Retroviral Capsid", Trends Biochem Sci **41**, 410-420 (2016).
14 L. Deshmukh, C. D. Schwieters, A. Grishaev, R. Ghirlando, J. L. Baber and G. M. Clore. "Structure and Dynamics of Full-Length HIV-1 Capsid Protein in Solution", Journal of the American Chemical Society **135**, 16133-16147 (2013).
15 O. Pornillos, B. K. Ganser-Pornillos and M. Yeager. "Atomic-level modelling of the HIV capsid", Nature **469**, 424-427 (2011).
16 J. A. Briggs, J. D. Riches, B. Glass, V. Bartonova, G. Zanetti and H. G. Krausslich. "Structure and assembly of immature HIV", Proc Natl Acad Sci U S A **106**, 11090-11095 (2009).
17 S. D. Fuller, T. Wilk, B. E. Gowen, H. G. Kräusslich and V. M. Vogt. "Cryo-electron microscopy reveals ordered domains in the immature HIV-1 particle", Curr Biol **7**, 729-738 (1997).
18 L. A. Carlson, J. A. Briggs, B. Glass, J. D. Riches, M. N. Simon, M. C. Johnson, B. Muller, K. Grunewald and H. G. Krausslich. "Three-dimensional analysis of budding sites and released virus suggests a revised model for HIV-1 morphogenesis", Cell Host Microbe **4**, 592-599 (2008).
19 J. A. Briggs, M. N. Simon, I. Gross, H. G. Krausslich, S. D. Fuller, V. M. Vogt and M. C. Johnson. "The stoichiometry of Gag protein in HIV-1", Nat Struct Mol Biol **11**, 672-675 (2004).

20 I. Kucharska, P. Ding, K. K. Zadrozny, R. A. Dick, M. F. Summers, B. K. Ganser-Pornillos and O. Pornillos. "Biochemical Reconstitution of HIV-1 Assembly and Maturation", J Virol **94** (2020).
21 L. S. Ehrlich, B. E. Agresta and C. A. Carter. "Assembly of recombinant human immunodeficiency virus type 1 capsid protein in vitro", J Virol **66**, 4874-4883 (1992).
22 B. K. Ganser-Pornillos, U. K. von Schwedler, K. M. Stray, C. Aiken and W. I. Sundquist. "Assembly properties of the human immunodeficiency virus type 1 CA protein", J Virol **78**, 2545-2552 (2004).
23 G. Zhao, J. R. Perilla, E. L. Yufenyuy, X. Meng, B. Chen, J. Ning, J. Ahn, A. M. Gronenborn, K. Schulten, C. Aiken and P. Zhang. "Mature HIV-1 capsid structure by cryo-electron microscopy and all-atom molecular dynamics", Nature **497**, 643-646 (2013).
24 S. Li, C. P. Hill, W. I. Sundquist and J. T. Finch. "Image reconstructions of helical assemblies of the HIV-1 CA protein", Nature **407**, 409-413 (2000).
25 S. Mattei, B. Glass, W. J. Hagen, H. G. Kräusslich and J. A. Briggs. "The structure and flexibility of conical HIV-1 capsids determined within intact virions", Science **354**, 1434-1437 (2016).
26 J. A. Briggs, T. Wilk, R. Welker, H. G. Kräusslich and S. D. Fuller. "Structural organization of authentic, mature HIV-1 virions and cores", Embo j **22**, 1707-1715 (2003).
27 D. A. Jacques, W. A. McEwan, L. Hilditch, A. J. Price, G. J. Towers and L. C. James. "HIV-1 uses dynamic capsid pores to import nucleotides and fuel encapsidated DNA synthesis", Nature **536**, 349-353 (2016).
28 R. A. Dick, D. L. Mallery, V. M. Vogt and L. C. James. "IP6 Regulation of HIV Capsid Assembly, Stability, and Uncoating", Viruses **10** (2018).
29 D. L. Mallery, K. M. R. Faysal, A. Kleinpeter, M. S. C. Wilson, M. Vaysburd, A. J. Fletcher, M. Novikova, T. Böcking, E. O. Freed, A. Saiardi and L. C. James. "Cellular IP6 Levels Limit HIV Production while Viruses that Cannot Efficiently Package IP6 Are Attenuated for Infection and Replication", Cell Reports **29**, 3983-3996.e3984 (2019).
30 S. Campbell, R. J. Fisher, E. M. Towler, S. Fox, H. J. Issaq, T. Wolfe, L. R. Phillips and A. Rein. "Modulation of HIV-like particle assembly in vitro by inositol phosphates", Proc Natl Acad Sci U S A **98**, 10875-10879 (2001).
31 R. A. Dick, K. K. Zadrozny, C. Xu, F. K. M. Schur, T. D. Lyddon, C. L. Ricana, J. M. Wagner, J. R. Perilla, B. K. Ganser-Pornillos, M. C. Johnson, O. Pornillos and V. M. Vogt. "Inositol phosphates are assembly co-factors for HIV-1", Nature **560**, 509-512 (2018).
32 A. Yu, E. M. Y. Lee, J. Jin and G. A. Voth. "Atomic-scale characterization of mature HIV-1 capsid stabilization by inositol hexakisphosphate (IP6)", Sci Adv **6** (2020).
33 J. R. Perilla and K. Schulten. "Physical properties of the HIV-1 capsid from all-atom molecular dynamics simulations", Nat Commun **8**, 15959 (2017).
34 A. Yu, E. M. Y. Lee, J. A. G. Briggs, B. K. Ganser-Pornillos, O. Pornillos and G. A. Voth. "Strain and rupture of HIV-1 capsids during uncoating", Proceedings of the National Academy of Sciences **119**, e2117781119 (2022).
35 A. J. Pak and G. A. Voth. "Advances in coarse-grained modeling of macromolecular complexes", Current Opinion in Structural Biology **52**, 119-126 (2018).

36 J. M. A. Grime, J. F. Dama, B. K. Ganser-Pornillos, C. L. Woodward, G. J. Jensen, M. Yeager and G. A. Voth. "Coarse-grained simulation reveals key features of HIV-1 capsid self-assembly", Nat Commun **7**, 11568 (2016).
37 J. M. Grime and G. A. Voth. "Early stages of the HIV-1 capsid protein lattice formation", Biophys J **103**, 1774-1783 (2012).
38 A. J. Pak, J. M. A. Grime, A. Yu and G. A. Voth. "Off-Pathway Assembly: A Broad-Spectrum Mechanism of Action for Drugs That Undermine Controlled HIV-1 Viral Capsid Formation", J Am Chem Soc **141**, 10214-10224 (2019).
39 D. L. Mallery, A. B. Kleinpeter, N. Renner, K. M. R. Faysal, M. Novikova, L. Kiss, M. S. C. Wilson, B. Ahsan, Z. Ke, J. A. G. Briggs, A. Saiardi, T. Böcking, E. O. Freed and L. C. James. "A stable immature lattice packages IP(6) for HIV capsid maturation", Science advances **7**, eabe4716 (2021).
40 M. del Alamo, G. Rivas and M. G. Mateu. "Effect of macromolecular crowding agents on human immunodeficiency virus type 1 capsid protein assembly in vitro", J Virol **79**, 14271-14281 (2005).
41 Z. Yu, M. J. Dobro, C. L. Woodward, A. Levandovsky, C. M. Danielson, V. Sandrin, J. Shi, C. Aiken, R. Zandi, T. J. Hope and G. J. Jensen. "Unclosed HIV-1 capsids suggest a curled sheet model of assembly", Journal of molecular biology **425**, 112-123 (2013).
42 B. K. Ganser-Pornillos, M. Yeager and O. Pornillos. "Assembly and architecture of HIV", Adv Exp Med Biol **726**, 441-465 (2012).
43 M. Grättinger, H. Hohenberg, D. Thomas, T. Wilk, B. Müller and H. G. Kräusslich. "In vitro assembly properties of wild-type and cyclophilin-binding defective human immunodeficiency virus capsid proteins in the presence and absence of cyclophilin A", Virology **257**, 247-260 (1999).
44 S. Mattei, A. Flemming, M. Anders-Össwein, H.-G. Kräusslich, J. A. G. Briggs, B. Müller and W. I. Sundquist. "RNA and Nucleocapsid Are Dispensable for Mature HIV-1 Capsid Assembly", Journal of Virology **89**, 9739-9747 (2015).
45 P. W. Keller, R. K. Huang, M. R. England, K. Waki, N. Cheng, J. B. Heymann, R. C. Craven, E. O. Freed and A. C. Steven. "A two-pronged structural analysis of retroviral maturation indicates that core formation proceeds by a disassembly-reassembly pathway rather than a displacive transition", J Virol **87**, 13655-13664 (2013).
46 G. A. Frank, K. Narayan, J. W. Bess, G. Q. Del Prete, X. Wu, A. Moran, L. M. Hartnell, L. A. Earl, J. D. Lifson and S. Subramaniam. "Maturation of the HIV-1 core by a non-diffusional phase transition", Nature Communications **6**, 5854 (2015).
47 X. Meng, G. Zhao, E. Yufenyuy, D. Ke, J. Ning, M. DeLucia, J. Ahn, A. M. Gronenborn, C. Aiken and P. Zhang. "Protease Cleavage Leads to Formation of Mature Trimer Interface in HIV-1 Capsid", PLOS Pathogens **8**, e1002886 (2012).
48 T. A. Bharat, N. E. Davey, P. Ulbrich, J. D. Riches, A. de Marco, M. Rumlova, C. Sachse, T. Ruml and J. A. Briggs. "Structure of the immature retroviral capsid at 8 Å resolution by cryo-electron microscopy", Nature **487**, 385-389 (2012).
49 J. Ning, G. Erdemci-Tandogan, E. L. Yufenyuy, J. Wagner, B. A. Himes, G. Zhao, C. Aiken, R. Zandi and P. Zhang. "In vitro protease cleavage and computer simulations reveal the HIV-1 capsid maturation pathway", Nature Communications **7**, 13689 (2016).

50 C. L. Woodward, S. N. Cheng and G. J. Jensen. "Electron cryotomography studies of maturing HIV-1 particles reveal the assembly pathway of the viral core", Journal of virology **89**, 1267-1277 (2015).
51 J. Liu, F. Sadre-Marandi, S. Tavener and C. Chen. "Curvature Concentrations on the HIV-1 Capsid", Computational and Mathematical Biophysics **3** (2015).
52 T. Thames, A. J. Bryer, X. Qiao, J. Jeon, R. Weed, K. Janicki, B. Hu, P. L. Gor'kov, I. Hung, Z. Gan, J. R. Perilla and B. Chen. "Curvature of the Retroviral Capsid Assembly Is Modulated by a Molecular Switch", The Journal of Physical Chemistry Letters **12**, 7768-7776 (2021).
53 S. J. Rihn, S. J. Wilson, N. J. Loman, M. Alim, S. E. Bakker, D. Bhella, R. J. Gifford, F. J. Rixon and P. D. Bieniasz. "Extreme Genetic Fragility of the HIV-1 Capsid", PLOS Pathogens **9**, e1003461 (2013).
54 A. I. Jewett, Z. Zhuang and J.-E. Shea. "Moltemplate a Coarse-Grained Model Assembly Tool", Biophysical Journal **104**, 169a (2013).
55 S. Plimpton. "Fast Parallel Algorithms for Short-Range Molecular Dynamics", Journal of Computational Physics **117**, 1-19 (1995).
56 E. Vanden-Eijnden and G. Ciccotti. "Second-order integrators for Langevin equations with holonomic constraints", Chemical Physics Letters **429**, 310-316 (2006).
57 J. D. Hunter. "Matplotlib: A 2D Graphics Environment", Computing in Science & Engineering **9**, 90-95 (2007).
58 W. Humphrey, A. Dalke and K. Schulten. "VMD: visual molecular dynamics", J Mol Graph **14**, 33-38, 27-38 (1996).
59 D. Stanzione, J. West, R. T. Evans, T. Minyard, O. Ghattas and D. K. Panda. in *Practice and Experience in Advanced Research Computing* 106–111 (Association for Computing Machinery, 2020).
60 J. Towns, T. Cockerill, M. Dahan, I. Foster, K. Gaither, A. Grimshaw, V. Hazlewood, S. Lathrop, D. Lifka, G. D. Peterson, R. Roskies, J. R. Scott and N. Wilkins-Diehr. "XSEDE: Accelerating Scientific Discovery", Computing in Science & Engineering **16**, 62-74 (2014).

Acknowledgements

The authors acknowledge the Texas Advanced Computing Center (TACC) at The University of Texas at Austin for providing HPC resources that have contributed to the research results reported within this paper.[59] This research also used the Extreme Science and Engineering Discovery Environment (XSEDE), which is supported by the National Science Foundation grant number ACI-1548562.[60]

Funding

This research was supported by the National Institute of Allergy and Infectious Diseases (NIAID) of the National Institutes of Health under grant R01 AI154092. A.J.P gratefully acknowledges support from the National Institute of Allergy and Infectious Diseases of the National Institutes of Health under grant F32 AI150477.

Author contributions: M.G., A.J.P and G.A.V. designed research. M.G. and A.J.P performed research. M.G. and A.J.P contributed methods, simulation code, and analytic tools. M.G., A.J.P., and G.A.V. analyzed data. M.G., A.J.P., and G.A.V. wrote the paper.

Competing interests: None

Data and materials availability:

All data needed to evaluate the conclusions in the paper are present in the paper and/or the supplementary Materials. All relevant data are available from the authors on request.